

Computational identification of Ga-vacancy related electron paramagnetic resonance centers in β -Ga₂O₃

Dmitry Skachkov and Walter R. L. Lambrecht
*Department of Physics, Case Western Reserve University,
10900 Euclid Avenue, Cleveland, OH-44106-7079, U.S.A.*

Hans Jürgen von Bardeleben
*Sorbonne Universités, UPMC Université Paris 06, UMR7588,
Institut des Nanosciences de Paris, 4 place Jussieu, 75005 Paris, France*

Uwe Gerstmann
Lehrstuhl für Theoretische Materialphysik, Universität Paderborn, 33098 Paderborn, Germany

Quoc Duy Ho and Peter Deák
*Bremen Center for Computational Materials Science,
University of Bremen, P.O. Box 330440, D-28334 Bremen, Germany*

A combined experimental/theoretical study of the electron paramagnetic centers in irradiated β -Ga₂O₃ is presented. Four EPR spectra, two $S = 1/2$ and two $S = 1$, are observed after high-energy proton or electron irradiation. Three of them have been reported before in neutron irradiated samples. One of the $S=1/2$ spectra (EPR1) can be observed at room temperature and below and is characterized by the spin Hamiltonian parameters $g_b = 2.0313$, $g_c = 2.0079$, $g_{a^*} = 2.0025$ and a quasi isotropic hyperfine interaction with two equivalent Ga neighbors of ~ 14 G on ⁶⁹Ga and correspondingly ~ 18 G on ⁷¹Ga in their natural abundances. The second (EPR2) is observed after photoexcitation (with threshold 2.8 eV) at low temperature and is characterized by $g_b = 2.0064$, $g_c = 2.0464$, $g_{a^*} = 2.0024$ and a quasi isotropic hyperfine interaction with two equivalent Ga neighbors of 10 G (for ⁶⁹Ga). A spin $S = 1$ spectrum with a similar g-tensor and a 50% reduced hyperfine splitting accompanies each of these, which is indicative of a defect of two weakly coupled $S = 1/2$ centers. Density functional theory calculations of the magnetic resonance fingerprint (g -tensor and hyperfine interaction) of a wide variety of native defect models and their complexes are carried out to identify these EPR centers in terms of specific defect configurations. The EPR1 center is proposed to correspond to a complex of two tetrahedral $V_{\text{Ga}1}$ with an interstitial Ga in between them and oriented in a specific direction in the crystal. This model was previously shown to have lower energy than the simple tetrahedral Ga vacancy and has a $2 - /3 -$ transition level higher than other V_{Ga} related models, which would explain why the other ones are already in their diamagnetic $3 -$ state and are thus not observed if the Fermi level is pinned approximately at this level. The EPR2 spectra ($S = 1/2$ as well as the related $S = 1$) are proposed to correspond to the octahedral $V_{\text{Ga}2}$ in which the spin is located on an oxygen off the defect's mirror plane and has a tilted spin density. Models based on self-trapped holes and oxygen interstitials are ruled out because they would have hyperfine interaction with more than two Ga nuclei and because they can not support a corresponding $S = 1$ center.

I. INTRODUCTION

Monoclinic β -Ga₂O₃ has recently attracted attention as an ultra-wide-band-gap semiconductor.¹ Its band gap of about 4.7 eV²⁻⁶ combined with unintentionally doped semiconducting rather than insulating properties make it attractive for high-power electronics applications. Mostly, the wide band gap leads to a high breakdown field (estimated to be possibly as high as 8 MV/cm based on the relation between band gap and break down voltage in other materials, and already demonstrated⁷ to be as high as 3.8 MV/cm), plays an important role in various figures of merit (FOM) for high-power transistor design, such as Baliga's FOM.⁸ Its good transparency in the ultraviolet region also make it suitable as a transparent conductor.⁹ The origin of unintentional doping and the limitations on the degree of n-type doping that can be achieved de-

pends on a thorough understanding of the defect physics. While a substantial amount of work¹⁰⁻²⁴ has already appeared on the defect physics, the experimental signatures of many of the defects are still unclear.

Recently, an Electron Paramagnetic Resonance (EPR) center was reported by Kananen *et al.*²² in neutron irradiated samples and ascribed to the octahedral Ga-vacancy site. In β -Ga₂O₃ there are two nonequivalent Ga sites one with a tetrahedral coordination ($\text{Ga}_{(1)}$) and one with an octahedral coordination ($\text{Ga}_{(2)}$).²⁵ Likewise, there are three distinct O sites, $\text{O}_{(1)}$ and $\text{O}_{(2)}$ are each connected to three Ga while $\text{O}_{(3)}$ is connected to four Ga (see Fig. 1).

Here we present an EPR study of β -Ga₂O₃ with defects introduced by high energy particle irradiation combined with first-principles calculations of the hyperfine interaction (HFI) and gyromagnetic g -tensors. A similar

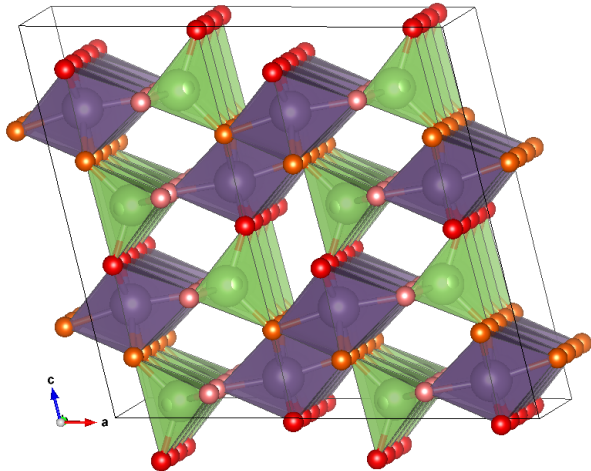


FIG. 1. Crystal structure of β -Ga₂O₃ shown in the 160 atom supercell indicating the polyhedra surrounding tetrahedral Ga₍₁₎ (in green) and octahedral Ga₍₂₎ (purple). The O₍₁₎, O₍₂₎, O₍₃₎ are colored coded as red, pink and orange.

spectrum to that of Ref. 22 is observed after irradiation in the dark. After photoexcitation a different center appears with different orientation of the main g -tensor axes and slightly smaller HFI-values. That EPR center has properties similar to those previously ascribed to the self-trapped hole (STH),²³ which similarly has spin density localized on an oxygen p -orbital but would not involve a Ga-vacancy. It was previously observed after X-ray irradiation at low temperature on already neutron irradiated samples. Two distinct $S = 1$ spectra are also reported here. The first of these, related to EPR1, was previously reported,²² the second, related to EPR2, was not. The characteristic g -tensors and hyperfine splitting of these centra and their thermal stability are presented.

Second, we present first-principles calculations for a wide variety of native defect models with the goal of identifying the chemical nature of the observed defect centers. The paper is organized as follows. We first present our computational methodology in Sec. II and give details of the experiment in Sec. III. Next, we present the experimental results in Sec. IV. Additional information on the experiments can be found in a brief prior report of this work.²⁴ The models investigated and the reasons why are described in Sec. V, followed by a presentation of the computational results in Sec. VI. We present a thorough comparison of the experimental results with calculations in Sec. VII and from it deduce the most likely models. A summary completes the paper.

II. COMPUTATIONAL METHODS

Density functional theory (DFT) is used in this work to first relax the structure of the models and determine

their transition levels. Subsequently the EPR parameters are calculated using the Gauge Including Projector Augmented Wave (GIPAW) method.

For a proper description of the strongly localized electron in the oxygen dangling bonds, structural relaxation of the models has been done with the hybrid functional^{26–28} with the parameters chosen as in Ref. 15. Specifically, the fraction of non-local exchange was $\alpha = 0.26$ with screening parameter $\mu = 0.00$.¹⁵ These parameters were determined in that paper to optimize both the band gap and satisfaction of the Generalized Koopmans Theorem (GKT) for various defects. They are in fact very close to the original PBE²⁶ parameters. This portion of the work used the Vienna Ab-initio Simulation Package (VASP).^{29–31} The same methodology as in Ref. 15 was also used to find the transition levels of the defects including details of the image charge corrections for charged states of the defect. In fact, for the models already studied in Ref. 15 we use the results directly from that paper while for the additional models the same methodology was followed here.

The GIPAW method^{32,33} uses self-consistent density functional perturbation theory to calculate the linear magnetic response of the defect system to an external magnetic field and is used here in its implementation included in the Quantum Espresso package.³⁴ The determination of the g -tensor via the GIPAW method is presently restricted to (semi-)local functionals: The non-local exact-exchange terms specific to hybrid functional are not yet included in the g -tensor code. Thus, we used a combined approach, where the structures previously relaxed within hybrid functional are then kept fixed and their electronic structure is recalculated at the GGA level using the Perdew-Burke-Ernzerhof (PBE)³⁵ functional and the wave functions and spin-densities obtained in this manner are then used to evaluate the g -tensor using the GIPAW code. We found that once the structure is relaxed with hybrid functional, the spin density recalculated with GGA-PBE without the hybrid functional terms is quite similar to the hybrid functional one and stays well localized on a single oxygen in all models we investigated. Thus, this approach should be adequate to determine the g -tensor.

A few comments are in order here on the accuracy with which we expect to be able to predict g -tensors. Agreement between calculated and experimental data for the principal values of the g -tensor is obtained typically to better than 0.0003 at the semilocal DFT level.^{33,36–40} However these errors are on a small g -tensor shift from the free-electron value and amount to a relative error of 30 %. In some cases, such as the Jahn-Teller distorted split interstitial (N-N_N⁰) in GaN the deviation for a single specific directions was 0.007.³⁷ All these defects have well localized spins already at the GGA level. There is not much experience yet with g -tensor calculations for acceptor type defects for which the localization of the spin is sensitive to the functional because of self-interaction errors, as is the case here. Thus, we estimate a conserva-

tive error bar of 0.01 on the larger Δg -tensor components. Therefore, to achieve our main goal of identifying the defect centers responsible for the observed EPR spectra, we prefer to focus on the qualitative aspects of the g -tensor, such as the ordering of the principal value directions.

As far as the hyperfine interaction both the VASP and GIPAW program were used. This part of the GIPAW program does not require the phase factors related to gauge-inclusion. The hyperfine tensor A consists of the isotropic Fermi-contact term, which essentially requires calculating the spin density at the relevant nuclear sites which carry a nuclear spin, which involves the s -like part of the wavefunctions on these sites only. In the present case, this corresponds to the Ga sites only because O has an isotope without nuclear spin with more than 99.9% abundance. We are thus dealing with superhyperfine (SHF) interaction. As expected, the SHF interaction is predominantly isotropic both in the computations and experiment. Therefore, we focus on the Fermi contact term and on the number of Ga atoms which exhibit a strong hyperfine interaction.

Within the VASP code we use the hybrid functional calculated spin density. It was found that the hybrid functional overestimates the experimental values by about a factor 2 for the V_{Ga} based models. The Fermi contact term clearly is very sensitive to the degree of localization of the defect wave function. Compared to the PBE-GGA result, we found that the wave function became a bit more localized in hybrid functional but it becomes more localized on both the O and the Ga and thereby in fact slightly increases the HFI.

Although the hybrid functional was specifically designed to satisfy the GKT and is thus already expected to describe the *overall* localization accurately, we should note that in calculations of the hyperfine interaction, we are placing a higher demand on the accuracy of the wave functions at the individual nuclei. The GKT requires linear dependence of the total energies as function of occupation number of the defect state and focuses on energy but for hyperfine it is the wave function itself that matters. It must have the right shape and distribution over O and its Ga neighbors and the right amount of $Ga-s$ character. We therefore also considered the DFT+ U approach and studied how different values of U affect the HFI. DFT+ U is often used to mimic the effects of non-local exchange of hybrid functionals. In the present case, the defect wave functions are primarily $O-p$ orbital derived and hence applying on-site Coulomb or Hubbard U terms on the $O-p$ orbitals may be expected to make the spin-density related to the $O-p$ hole in the EPR active state more localized on $O-p$. We should point out here that we apply such U terms on all O but it affects mainly the localization of the particular O on which the hole is localized because the empty states in DFT+ U are affected differently from the filled ones. We find indeed that using this DFT+ U approach with U on $O-p$ provides relaxed structures similar to hybrid functional. This is because the localization of the spin on a single

atom is accompanied by related structural distortion via a feedback loop. Thus the DFT+ U method can be used as an alternative to hybrid functional to obtain realistic structural models for these defects.

However, *a-priori* it is not clear whether this DFT+ U approach would also increase the spin-density on the neighboring Ga or reduce it. We find, in fact, that it pulls weight away from the Ga toward the O and hence reduces the HFI on the Ga atoms. We estimated the size of U using the linear response approach proposed by Cococcioni and de Gironcoli^{41,42} for some of the simple V_{Ga} defects and found values of about $U \approx 6 - 7$ eV. For another defect with spin on a neighboring oxygen, Mg_{Ga} , the HFI calculated within hybrid functional⁴³ or pure PBE agree well with experiment without adding U terms. Both a Mg_{Ga} and a V_{Ga} , present a repulsive potential which pushes out a state above the valence band and which is thus $O-p$ -like. However, one still expects it to have more of a dangling bond character for V_{Ga} than for Mg_{Ga} . Interstitial O_i also correspond to O -localized spins and are considered here and found to have somewhat smaller HFI on their neighboring Ga than V_{Ga} within the same functional. We thus conclude that a single U value or hybrid functional may not be optimal for all defects. In the results below, we will start from a somewhat conservative value of $U = 4$ eV used for all models to allow a consistent comparison and discuss how the results change with U although we do not propose to simply adjust U until agreement is obtained. Instead we base our conclusions on identifying models mostly on qualitative aspects, namely how many Ga atoms have significant hyperfine interaction.

We have also considered another possible reason for the overestimate of the HFI. For both EPR1 and EPR2 the most promising models turn out to undergo a symmetry breaking. In the EPR1 case, it corresponds to a complex consisting of two vacancies and an interstitial in between them which has an inversion center. For EPR2, the defect has a mirror plane. The spin could thus be on either side of the defect but is found to be localized on one side. However, we may now consider that this symmetry breaking could undergo a dynamic Jahn-Teller effect. In other words, there is a coupling to a local vibrational mode which presents a double well potential energy landscape. When the atoms are displaced one way, the spin localizes on one side and vice versa. This is because of the feedback loop between localization and atomic displacements mentioned earlier. The spin would then flip back and forth between the two equivalent sides of the defect. The total wave function is then a product of the electronic wave function and the vibronic one and in calculating the probability of the electron to be on a given nucleus, which gives the hyperfine interaction, one would have to carry out an integral over the vibronic wave function modulo squared and take a thermal average over the vibronic states. Unfortunately, it is beyond the scope of the present work to evaluate this effect quantitatively. It nonetheless becomes clear that spin-phonon coupling

could lead to a dynamical reduction factor of the HFI. In a classical picture, the spin spends part of its time on one side and part of its time on the other side but also in transit between the two and hence in a less localized state so that ultimately the probability to find the spin at the nuclear sites is reduced. Such reduction factors due to dynamical Jahn-Teller effects have been discussed in literature before, for example in the paper by Ham⁴⁴ and in Mauger *et al.*⁴⁵. It would lead to a temperature dependent HFI, which has not yet been studied in detail but also could lead to an overall reduction.

In summary, although we will show below that the calculations overestimate the contact HFI, we do not view this as a crucial point in making our identification of the models. It is tentatively attributed to the difficulty in describing the wave function of dangling bond like acceptor states subject to strong self-interaction errors. Even though hybrid functionals and DFT+ U methods can remedy this problem partially, it is not yet clear that a single choice will describe different defects equally well. In addition, dynamical Jahn-Teller effects, not yet included in the first-principles framework may reduce these hyperfine factors and also affect spin-orbit coupling and g -tensors precise values.

Further details of the computational method are as follows. The defects were simulated using periodic boundary conditions in 160 and 240 atom supercells, which are respectively a $1 \times 4 \times 2$ and $1 \times 4 \times 3$ superlattices of the 20 atom conventional cell of the base-centered $C2/m$ -spacegroup β -Ga₂O₃ structure.²⁵ The plane wave expansion was used with a cut-off of 100 Ry and the Brillouin zone integration used the Γ -point only for the self-consistent calculations and hyperfine structure. Convergence was tested by also using a $2 \times 2 \times 2$ shifted mesh. For the g -tensor calculations, which are more sensitive to \mathbf{k} -point convergence, the $2 \times 2 \times 2$ mesh was used and convergence was tested by also using a $3 \times 3 \times 3$ mesh in a few test cases. Troullier-Martins type pseudopotentials obtained within the PBE exchange correlation functional were used.

The hyperfine parameters were calculated using the QE-GIPAW code⁴⁶ as well as the VASP code. The relativistic hyperfine tensor consists of the isotropic Fermi contact term which requires the spin density within a distance of the Thomas radius ($r_T = Ze^2/mc^2$) from the nuclear sites as well as the dipolar terms.⁴⁷ (Here, Z is the atomic number, e the elementary charge, m the free electron mass and c the speed of light.) Within a pseudopotential or projector augmented wave approach, a reconstruction of the all-electron wave functions from the pseudo wave functions is required.⁴⁸

III. EXPERIMENTAL DETAILS

Single crystals of n-type non-intentionally doped β -Ga₂O₃ have been purchased from a commercial supplier (Tamura, Japan). The sample thickness was 500 μm and

the size $4 \times 4 \text{ mm}^2$ with the \mathbf{b} -axis normal to the sample plane. The samples have been irradiated at room temperature with high energy electrons or protons to introduce intrinsic defects. Typical fluences were 10^{16} cm^{-2} . The irradiation conditions (12 MeV protons, 30 MeV electrons) were chosen so as to guarantee a homogenous defect formation in the entire sample volume and so that no hydrogen is introduced in the sample due to the irradiation. The EPR spectra were taken with an X-band spectrometer (resonant frequency 9.3 GHz) and a variable temperature (4K-300K) cryostat, which allowed in-situ optical excitation. Angular variations of the EPR spectra were measured in three crystal planes. In addition to the irradiation induced defect, the samples presented EPR spectra from a shallow donor and a weak Fe³⁺ spectrum, which were discussed in our previous report.²⁴

IV. EXPERIMENTAL RESULTS

In Fig. 2 we show the EPR spectra of the irradiation induced defect center for the applied magnetic field oriented $\mathbf{B} \parallel \mathbf{b}$ both before and after photoexcitation. We call these spectra respectively EPR1 and EPR2. EPR1 occurs in the dark already at room temperature. It displays a well-resolved multiplet structure which can be simulated by a spin $S = 1/2$ center, interacting with two equivalent Ga neighbors. Due to the presence of two Ga isotopes (⁶⁹Ga, ⁷¹Ga) both with nuclear spin $I = 3/2$ but different isotopic abundances (60.1%/39.9%) and different nuclear moments in these non isotopically modified samples, the hyperfine interaction gives rise to a characteristic lineshape structure (the simulation is shown in Fig. 2 as the black solid line). It clearly agrees with the spectrum reported previously by Kananen *et al.*²²

When the sample is photoexcited at low temperature ($T < 100 \text{ K}$) the spectrum EPR1 is erased and replaced by a different spectrum, EPR2, which is metastable up to a temperature of $T = 100 \text{ K}$, at which the EPR1 spectrum is regenerated. The angular variation of EPR1 and EPR2 in two planes is shown in Fig.3. Fig.4 shows the crystallographic directions relative to the sample. The main parameters extracted from the fit are summarized in Table I. The spectral dependence of the photoexcitation process was shown in Fig. 8 of Ref. 24 and shows the transition occurs rather abruptly for photon energies exceeding 2.8 eV.

The particular g -values and the superhyperfine interaction with two equivalent Ga neighbors indicate for both centers a defect localized on a single oxygen site with two nearest Ga neighbors and are thus most likely associated with Ga vacancy defects, which will be further substantiated by means of the calculations. The single spin $S = 1/2$ nature of the spectrum indicates the V_{Ga} is in the charge state $q = -2$. The various one electron levels in the gap closely above the valence band maximum (VBM) would be completely filled in the $q = -3$ charge state, so that the $q = -2$ charge state has a single hole.

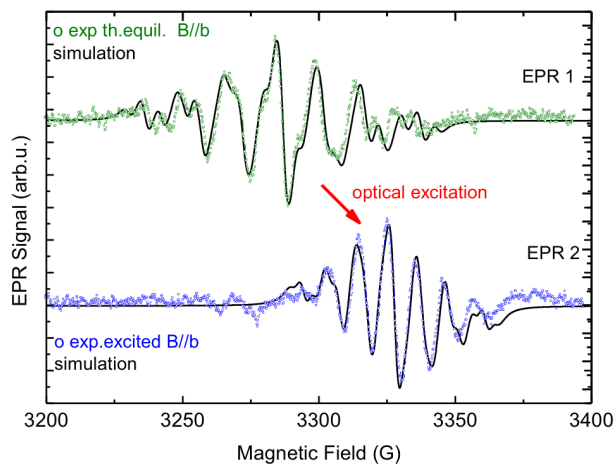


FIG. 2. Experimental and simulated EPR spectra in β -Ga₂O₃ for $\mathbf{B} \parallel \mathbf{b}$ before photoexcitation (green) at $T = 300$ K and after photoexcitation (blue) at $T = 52$ K.

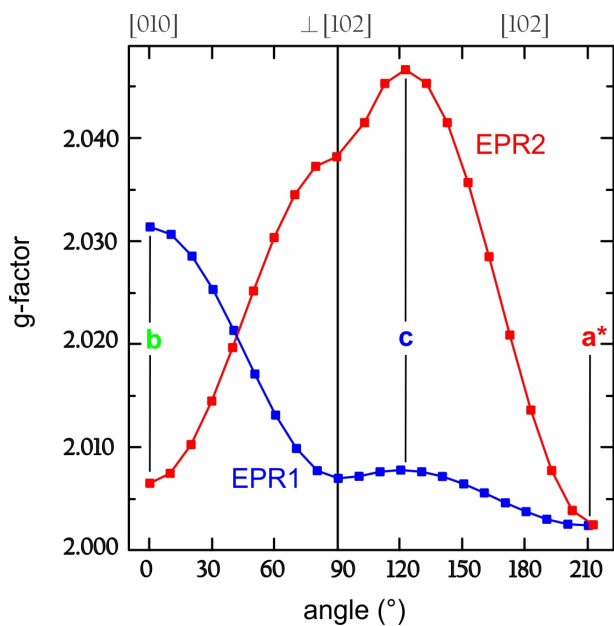


FIG. 3. Angular variation of the g -factor for the variation of the magnetic field in two crystal planes for EPR1 (before) and EPR2 (after) photoexcitation.

The O hyperfine is not seen because the ^{16}O isotope has no nuclear spin and is more than 99.9 % abundant. The ^{17}O isotope with a spin of $I = 5/2$ has a natural abundance of only 3.8×10^{-4} . The hyperfine splitting is thus really a superhyperfine splitting because it does not occur on the atom where the spin is dominantly localized but on its neighbors.

Each of the $S = 1/2$ spectra reported above is accompanied by a corresponding distinct $S = 1$ spectrum (see Fig. 5). While the first $S = 1$ spectrum related to EPR1 was also previously reported by Kananen²² we here emphasize that there are two distinct $S = 1$ spectra. Each

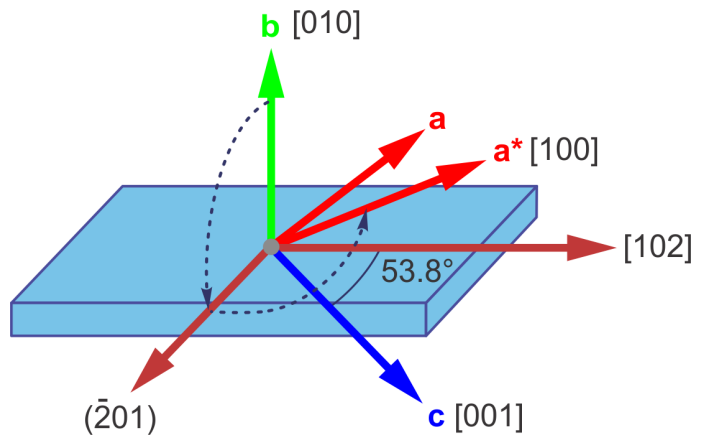


FIG. 4. Sample indicating crystal orientations. $[102]$ means $\mathbf{a} + 2\mathbf{c}$, while (-201) means $-2\mathbf{a}^* + \mathbf{c}^*$, where the starred vectors are reciprocal lattice vectors, so that (-201) is perpendicular to $[102]$. The dashed curved lines indicate the angular variation of the magnetic field in two planes used in Fig. 3. The angle between \mathbf{a} and \mathbf{c} is 103.7° .

TABLE I. EPR parameters g -tensor and hyperfine A tensor for ^{69}Ga ; \mathbf{b} , \mathbf{c} are the axes of the conventional unit cell, \mathbf{a}^* is the reciprocal lattice vector in the \mathbf{b} -plane at 90° from the \mathbf{c} -axis. These are close to the principal axes of the g -tensor. The HFI parameters for the ^{71}Ga are obtained by multiplying by the ratio of their gyromagnetic factors which is 1.27059. The zero field splitting parameter D corresponds to the corresponding $S = 1$ spectra.

Dark	
g_b	2.0313
g_c	2.0079
g_{a^*}	2.0025
A_b (G)	13.8
A_c (G)	14.6
A_{a^*} (G)	12.8
D (MHz)	250
Photoexcited	
g_c	2.0464
g_{a^*}	2.0024
g_b	2.0064
A_b (G)	9.8
A_c (G)	9.4
A_{a^*} (G)	9.0
D (MHz)	322

has a g -tensor equal to the corresponding $S = 1/2$ and a hyperfine splitting with about half the value of the contact hyperfine interaction for the $S = 1/2$. This indicates it consists of two weakly interacting $S = 1/2$ spins. It means that the same defect can exist in two charge states with either one or two holes. The spin Hamiltonian for the $S = 1$ case contains a term $\mathbf{S} \cdot \mathbf{D} \cdot \mathbf{S}$ which is usually written as

$$H = D[S_z^2 - S(S+1)] + E(S_x^2 - S_y^2) \quad (1)$$

with $D = \frac{3}{2}D_z$ and $E = \frac{1}{2}(D_x - D_y)$. Here, the zero-field

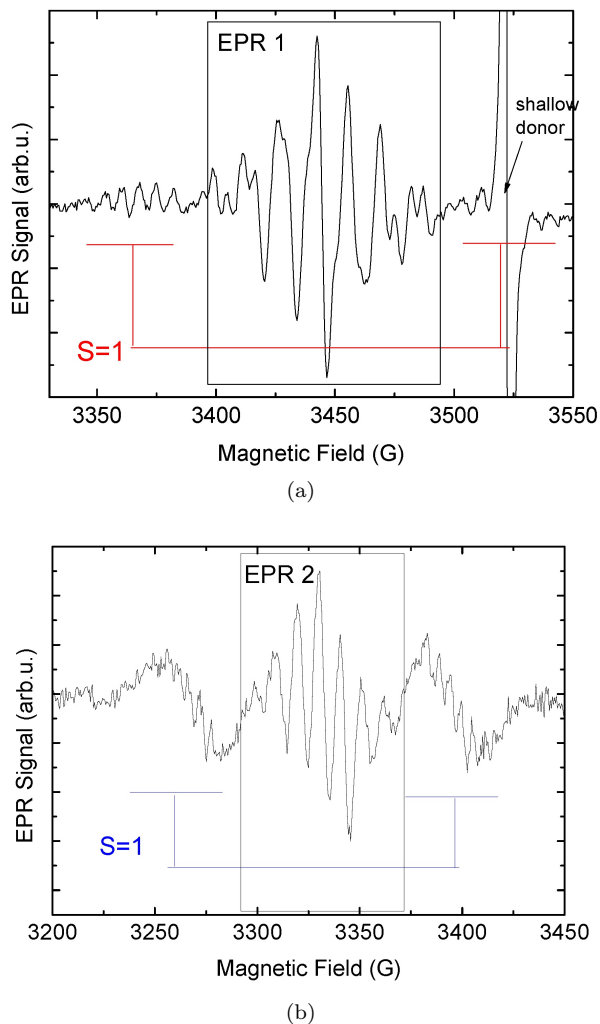


FIG. 5. $S = 1$ spectra accompanying the $S = 1/2$ (a) before photoexcitation for $\mathbf{B} \perp \mathbf{b}$ and (b) after photoexcitation for $\mathbf{B} \parallel \mathbf{b}$.

splittings are nearly axial with $E = 0$. Their D values are given in Table I. They have principal axes at 20° from the $[102]$ axis toward the \mathbf{c} -axis in the \mathbf{b} -plane for EPR1 and parallel to $[102]$ for EPR2.

V. COMPUTATIONAL MODELS

Under irradiation both vacancies and interstitials of both Ga and O atoms are likely to occur. However, we focus on Ga-vacancies and O-interstitials because only these are expected to have spin localized on an O atom, as is clearly established by the experiment.

The first models are: (M1) $V_{\text{Ga}1}$ with spin localized on $O_{(1)}$ neighbor, (M2) $V_{\text{Ga}2}$ with the spin localized on $O_{(2)}$ on the mirror-plane, (M3) a $V_{\text{Ga}2}$ with tilted spin localized on two $O_{(1)}$ on either side of the mirror plane. We will also refer to this as the “tilted spin” model. This model is the structure obtained in Ref. 15 as ground

TABLE II. Total energy differences (in eV) of Ga vacancies and their stoichiometrically equivalent complexes in different charge states relative to the $q = 0$ state of $V_{\text{Ga}1}$. These are calculated using the hybrid functional.

q	0	-1	-2	-3
$V_{\text{Ga}1}$	0	4.62	9.96	16.25
$V_{\text{Ga}2}$	0.68	4.77	9.84	15.67
$V_{\text{Ga}1} - \text{Ga}_{ic} - V_{\text{Ga}1}$	0.99	4.91	9.70	15.10
$V_{\text{Ga}1} - \text{Ga}_{ib} - V_{\text{Ga}1}$	0.33	3.89	9.38	15.54

state for the $V_{\text{Ga}2}$. The M2 model with the spin on the mirror plane $O_{(2)}$ can be stabilized when using a different initial displacement of the atoms. In hybrid functional calculations (with the same parameters as in Ref. 15) that model lies 0.27 eV higher in energy. Nonetheless we will also consider M2 for the purposes of comparing its EPR parameters with experiment, in particular because it corresponds to the model proposed by Kananen *et al.*²² for EPR1.

As for model M3, it should be pointed out that in this model the wave function tends to become asymmetric with spin localized on one $O_{(1)}$ on one side of the mirror plane. However, two variants exist: a left, and a right one, and the experiment which averages macroscopically over many centers in the sample, would then see an average of the two. Alternatively, the spin may dynamically flip back and forth between the two sides in the same defect on the time scale of the experiment. This would correspond to a dynamic Jahn-Teller distortion. As a convenient way to calculate the g -tensor for this titled spin model, we have enforced the symmetry in the calculation with the single spin distributed equally over the two sides. While this would then seem to entail hyperfine interaction with 4 instead of 2 Ga, or rather two slightly inequivalent pairs, we should keep in mind that the spin is not really spread over the two sides but temporarily on one or the other in a dynamic sense. Thus it still only interacts with two Ga at any given moment. Please note that either of the two approaches, averaging the left and right variants of the unsymmetrized model M3 or the symmetrized M3 will give the same g -tensor.

Next, we consider complexes such as the $V_{\text{Ga}1} - \text{Ga}_{ib} - V_{\text{Ga}1}$ complex, which we label M4. We will refer to it as the (b)-complex for short. Figures of the models including the results of the spin density appear in the next section. These type of complexes were found to have lower energy than a simple $V_{\text{Ga}1}$ by Varley *et al.*¹⁰ in their most negative charge state and could occur by means of a Ga diffusion process.⁴⁹ There are actually two nonequivalent such complexes, as defined in Fig. 4 of Kyrtos *et al.*⁴⁹. The M4 model corresponds to the one indicated as the (b) location of the interstitial Ga. The two $O_{(1)}$ on which the spins localizes and which are related by a center of inversion at the (b)-interstitial site in this case have each two $\text{Ga}_{(2)}$ neighbors. In the other case, indicated by (c) in Fig. 4 of Ref. 49 the spins localize on $O_{(3)}$ type

atoms which have each three Ga neighbors. Our total energy calculations using the hybrid functional¹⁵ (shown in Table II) indicate that this (c)-complex has the lowest energy among the complexes for the $q = -3$ charge. However, for the EPR relevant charge states $q = -2$ and $q = -1$ the (b)-complex has the lowest energy. We will later discuss their likelihood of being in the $q = -2$ or $q = -1$ charge states which are relevant as EPR active states. We will refer to the (c)-complex as the M5 model. Another complex consists of $V_{\text{Ga1}} - \text{Ga}_{ia} - V_{\text{Ga2}}$ is called the M6 model.

We found for the M4 complex that the spin stays localized on one $\text{O}_{(1)}$ similar to the simple V_{Ga1} model and as a result exhibits slightly different relaxation near each V_{Ga1} in the model. Obviously there are then two variants but their g -tensors are exactly the same because they are related by an inversion symmetry. Thus no averaging is required. These models were initially relaxed with the DFT+ U method but later checked with hybrid functional when their transition levels were determined. We note, that similar to M3 we could here also have symmetrized the model explicitly, but we find that this makes little difference and hence we do not show the results for the symmetrized version here.

The above models focused on Ga-vacancies. However, in a previous work,²³ the self-trapped hole was proposed as a model for EPR2. We consider two self-trapped hole (STH) models with the hole trapped either on $\text{O}_{(1)}$ ^{11,15} (M7) or on two $\text{O}_{(2)}$ (M8).¹⁵ The site on which the hole is trapped is determined by the initial displacement of the neighboring atoms from which the system converges to the closest local minimum in the energy. So, there can indeed be different hole trapping sites and hopping between them could occur at higher temperature. The M8 model has two $\text{Ga}_{(2)}$ and one $\text{Ga}_{(1)}$ neighbor. If the $\text{Ga}_{(1)}$ were far enough removed due to the relaxations around the hole, then it could be a plausible model for the EPR centers at hand. However, we will show that this is not the case and that the hyperfine on the third Ga is actually higher than the first two. The M8 model has already spin distributed over two $\text{O}_{(2)}$ atoms and is thus likely to cause hyperfine on more Ga. We find below that this is indeed the case and this rules out that model. Self-trapping on $\text{O}_{(3)}$ was not found to occur in previous studies.¹⁵

Another type of defect which is expected to have spin density localized on oxygen is interstitial oxygen, O_i . The latter adopts a split interstitial configuration. It consists of an O_2 dumbbell on a lattice O-site. Among such models, the O_2 located on the $\text{O}_{(1)}$ site is the most promising. In fact, in the neutral charge state, it was found to be oriented close to the \mathbf{c} direction. A metastable state occurs when a hole is added to this defect in this configuration. We label this model as M9. We should mention that the model for this metastable state was obtained here using the DFT+ U approach rather than the hybrid functional. However, a previous work¹⁵ at the hybrid functional level also found a split interstitial O_i ; the transition levels of

which will be discussed later in sec. VII, A. Eventually, its ground state has the dumbbell rotated closer to the \mathbf{b} direction. However, the \mathbf{c} -oriented dumbbell with single hole spin located on it was here considered *a-priori* as an attractive model to explain EPR2 because the spin might become more localized near one of the two O and thereby have reduced hyperfine interaction with the third Ga, which is a $\text{Ga}_{(1)}$ and because it was likely to have its g -tensor along \mathbf{c} . As a final related system, we consider the $\text{O}_i - V_{\text{Ga1}}$ complex in which that $\text{Ga}_{(1)}$ is removed. This is labeled the M10 model. It was relaxed within DFT+ U .

VI. COMPUTATIONAL RESULTS

The g -tensors principal values and axes as well as the HFI splittings are summarized in Table III for Ga-vacancy related models (M1-M6) and in Table IV for the self-trapped and interstitial O related models (M7-M10).

The spin density, g -tensor and atoms with large HFI are shown in two views for V_{Ga1} (M1) in Fig. 6 and for V_{Ga2} (M2) in Fig. 7. The results for the $V_{\text{Ga1}} - \text{Ga}_{ib} - V_{\text{Ga1}}$ complex (M4) is shown in Fig. 8 while those of M5, M6 are shown in Supplementary Information.⁵⁰

VII. DISCUSSION

A. Models for EPR1

We now compare the calculated results with the experimental results. Starting with the simple V_{Ga} models, we first note that both V_{Ga1} and V_{Ga2} in the M2 model, have the main g -tensor component along the \mathbf{b} direction in agreement with the experimental data for EPR1. The g -tensor however differs from the experimental one in two respects: first, the calculated one has a large, an intermediate and a small principal values, whereas the experimental one has only one large Δg and two close significantly smaller values. Second, the smallest g principal value direction in the calculation is close to \mathbf{c} (within about 20°), while in the experiment it is along \mathbf{a}^* .

The direction of the smallest g -component can be seen to correspond to the direction of the p -like spin density (see *e.g.* Fig. 7). This in fact makes sense from a perturbation theory point of view and in the empirical model used in Kananen *et al.*²². In a simple perturbation theory picture, the Δg arises from cross-terms between the orbital Zeeman $\mathbf{B} \cdot \mathbf{L}$ and spin-orbit coupling $\mathbf{S} \cdot \mathbf{L}$ terms, which lead to an effective $\mathbf{B} \cdot \mathbf{S}$ term and hence a change in the gyromagnetic factor in the spin Zeeman term,

$$\Delta g_{ij} \propto \sum_n \frac{\langle 0 | L_i | n \rangle \langle n | L_j | 0 \rangle}{E_n - E_0}, \quad (2)$$

where $|0\rangle$ is the one-electron state with unpaired spin and $|n\rangle$ all other states. If we pick the direction of the spin

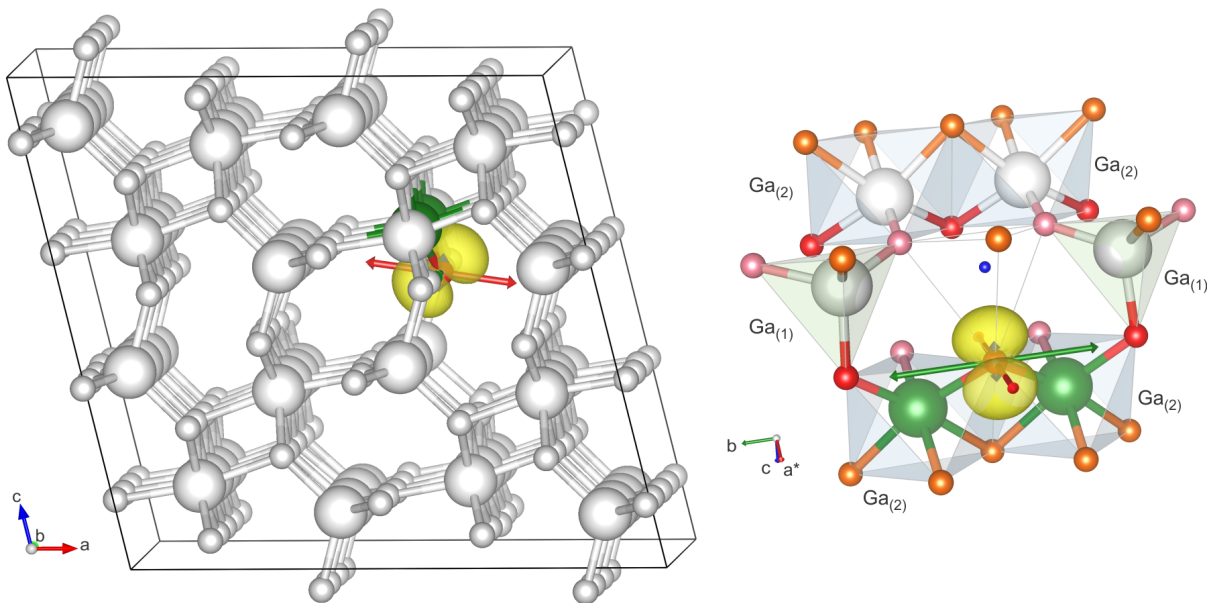


FIG. 6. V_{Ga1} (M1) structure, spin density in yellow, g -tensor principal axes indicated by double arrows with length proportional to the Δg (deviation from free electron value $g_e = 2.002391$), green colored Ga atoms are the ones with strong HFI. On the left it is viewed in the supercell, on the right the local structure is viewed from a different angle, the small O spheres are color coded red O₍₁₎, pink O₍₂₎, orange O₍₃₎ and the polyhedra surrounding the Ga and their type are indicated. The tetrahedral vacancy V_{Ga1} is indicated as a colorless tetrahedron with a small blue sphere.

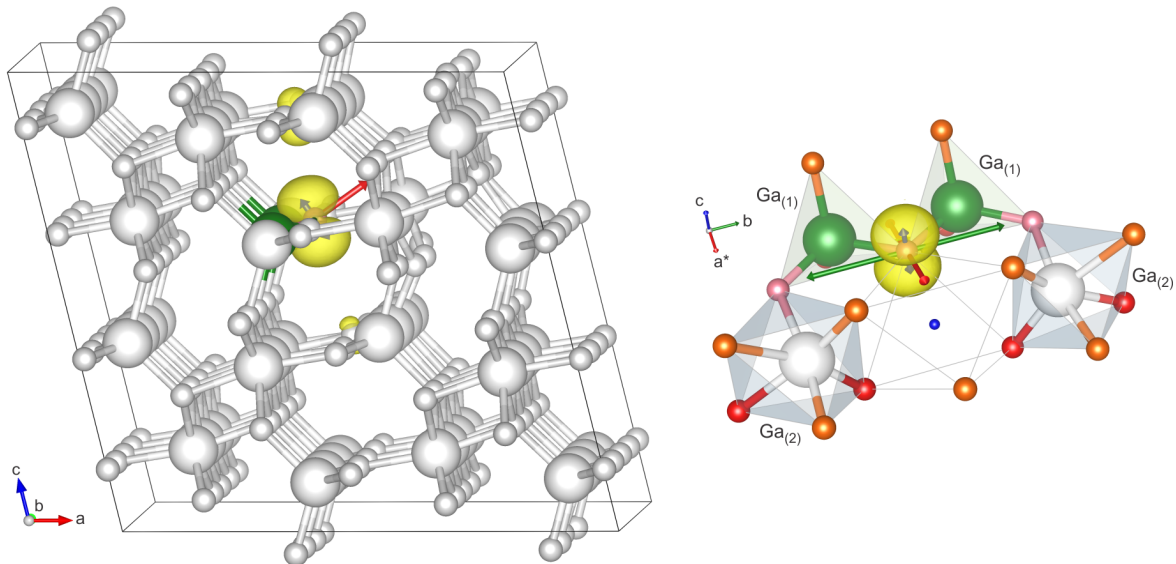


FIG. 7. V_{Ga2} (M2) structure, spin density in yellow, g -tensor and Ga atoms with strong HFI. See Fig. 6 for details.

density as the p -orbital momentum quantization axis z , then the angular momentum matrix elements involving L_z are zero and give no contribution for the g_{zz} , *i.e.* the deviation from the free electron value $g_e \approx 2.002319$, in that direction whereas in the orthogonal directions, matrix elements of L_+ and L_- enter and can give a non-zero Δg . Furthermore, we can see that the highest Δg occurs along the direction of the line that joins the two Ga atoms with strongest HFI. This indicates that the

O p -orbital spread in this direction contributes more to close lying excited states. Of course, this is only a rough guide because the eigenstates of the defect are not purely O p -states.

In spite of the shortcomings in the comparison of theory and experiment mentioned above and considering the uncertainties in Δg and its principal directions for the smaller Δg components, it is remarkable that both types of Ga vacancies give very similar results and in reason-

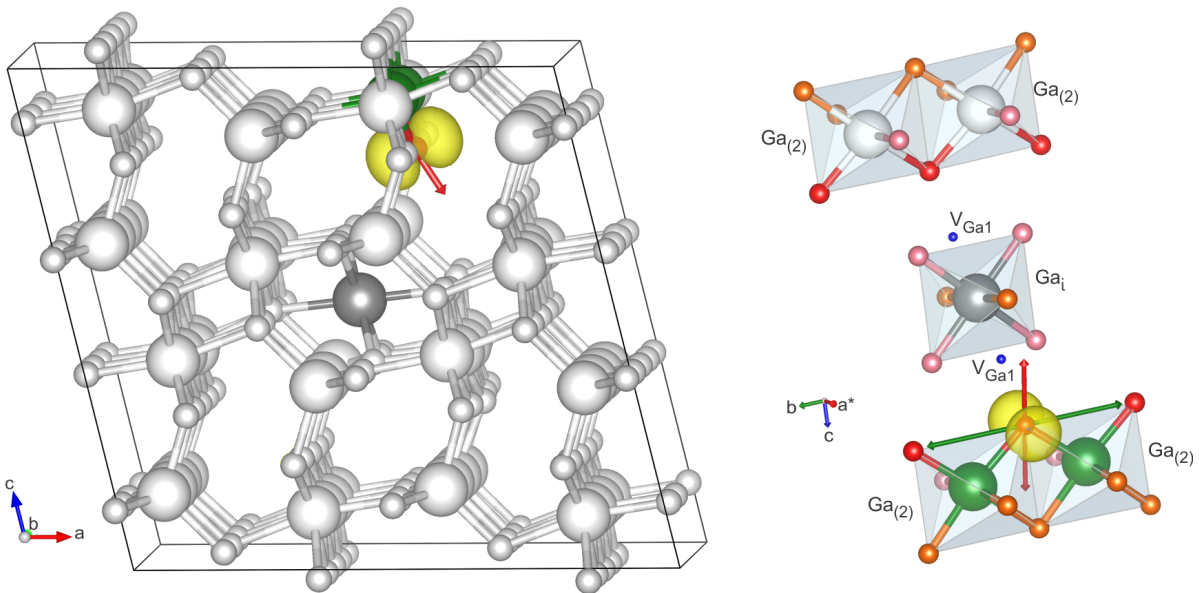


FIG. 8. $V_{\text{Ga}1} - \text{Ga}_{ib} - V_{\text{Ga}1}$ (M4) structure, spin density in yellow, g -tensor principal axes (green is larger component, red intermediate) and Ga atoms with strong HFI. Details as in Fig. 6.

able agreement with the major features of the experiment. This already strongly indicates a Ga-vacancy as basic model for EPR1. We will further refine the model below but first briefly discuss the hyperfine splitting for these models.

The hyperfine splitting for both of these models is on the two equivalent Ga atoms that are connected to the spin-carrying O. The fact that the hyperfine is on two Ga neighbors agrees with experiment but its value depends strongly on the functional used as already mentioned in Sec.II. Within pure PBE-GGA, its value is significantly overestimated (about -29 G). With hybrid functional it is even larger, namely -32 G. Within DFT+ U , the value depends strongly on U . For $U = 4, 8, 10$ eV its values are respectively $-22, -17, -16$ G. So, they become smaller with increasing U , but even for $U = 10$ eV they are still somewhat overestimated. A value of $U > 10$ eV appears unreasonable, so this indicates that the + U approach is still imperfect to describe the spread and shape of the wave function or that other effects not included at this point, such as dynamic Jahn-Teller effects or correlation effects not captured by DFT are required. The other possibility is, of course, that we have not yet found the correct model, but, as can be seen from Table III all vacancy related models have hyperfine interactions of the same order of magnitude.

Next, we consider the various Ga-vacancy-pair Ga-interstitial complexes (models M4-M6, see also Fig. 8 and Supplementary Information⁵⁰). Among these, it is clear that only M4 gives reasonable agreement with experiment. M5 has hyperfine interaction with three Ga and its g -tensor has two almost equal large values 0.018 along \mathbf{b} and \mathbf{a}^* in disagreement with both EPR1 and

EPR2. M6 has its largest value along \mathbf{a}^* , the spin spread over two equivalent $\text{O}_{(2)}$ and significantly different hyperfine on two pairs of Ga. In contrast, M4 (Fig. 8) has a g -tensor maximum value along \mathbf{b} , the next along \mathbf{c} and the smallest along \mathbf{a}^* , in agreement with the experiment. Furthermore, we may consider this as the actual ground state of the $V_{\text{Ga}1}$, since it has lower energy than a simple $V_{\text{Ga}1}$ and is formed from the latter by a simple migration of a lattice Ga toward an interstitial position. Finally, in this model, as mentioned in Sec. II we may have to consider a dynamic Jahn-Teller situation where the symmetry breaking occurs dynamically and the spin flips back and forth between the two sides of the defect complex, which may introduce a hyperfine reduction factor. This would help to correct the HFI overestimate for this model but not for the single vacancies.

Our conclusion thus far is that the M4 double vacancy-interstitial complex is the best fitting model for EPR1. However, one expects that during irradiation vacancies on both tetrahedral ($\text{Ga}_{(1)}$) and octahedral ($\text{Ga}_{(2)}$) site are equally likely. Thus we need to address next why among the V_{Ga} models only vacancies on the $\text{Ga}_{(1)}$ sublattice would be seen in experiment. In n -type conducting $\beta\text{-Ga}_2\text{O}_3$ the V_{Ga} are expected to be all in the diamagnetic $q = -3$ charge state, with all the O-dangling bond like states near the VBM completely filled, while an EPR active $S = 1/2$ state requires $q = -2$. The Fermi level position in equilibrium was estimated in Ref. 15. After irradiation, equilibrium no longer applies and the Fermi level is expected to shift to a position lower in the gap. From the presence of the Fe^{3+} EPR and the relation of Fe^{3+} with a Deep Level Transient Spectroscopy (DLTS) level at 0.78 eV below the CBM¹⁶ we know it

TABLE III. Calculated EPR parameters for various Ga-vacancy related models (labeled M1 to M6), the O on which the spin is localized in column 2. The g -tensor is given by Δg_i (difference from the free electron g -value) and principal values ordered from high to low; the corresponding axes are specified by their polar angle θ_i from the $\hat{\mathbf{z}} = \mathbf{b}$ axis and azimuthal angle ϕ_i from the $\hat{\mathbf{x}} = \mathbf{a}^*$ axis, both in $^\circ$, followed by which crystal axes are closest to these directions. For the hyperfine interaction HFI, the number of Ga atoms with strong HFI and the isotropic component of the A tensor (in $10^{-4}\text{T}=\text{Gauss}$) is given for the ^{69}Ga isotope. Note that these HFI are from PBE+ U wave functions with $U = 4$ eV; for further discussion of the U dependence see text. For comparison the corresponding data of the experimentally observed $S = 1/2$ spectra is also given (first two lines).

Model	O	g -tensor			HFI	
label structure	type	Δg_1 θ_1 ϕ_1	Δg_2 θ_2 ϕ_2	Δg_3 θ_3 ϕ_3	#Ga	A (G)
EPR1		0.0289 b	0.0056 c	0.0002 a_*	2	13.7
EPR2		0.0441 c	0.0041 b	0.0001 a_*	2	9.4
M1 $V_{\text{Ga}1}$	$O_{(1)}$	0.0219 0 b	0.0175 90 a_*	0.0045 90 c	2	-22
M2 $V_{\text{Ga}2}$	$O_{(2)}$	0.0235 0 b	0.0161 90 a_*	0.0062 90 c	2	-22
M3 $V_{\text{Ga}2}$	$O_{(1)}$	0.0349 88 c	0.0180 80 a_*	0.0160 10 b	2 2	-21 -16
M4 $V_{\text{Ga}1} - \text{Ga}_{ib} - V_{\text{Ga}1}$	$O_{(1)}$	0.0228 0 b	0.0124 90 c	0.0025 90 a_*	2	-21
M5 $V_{\text{Ga}1} - \text{Ga}_{ic} - V_{\text{Ga}1}$	$O_{(3)}$	0.0187 0 b	0.0177 90 a_*	0.0036 90 c	2 1	-21 -20
M6 $V_{\text{Ga}1} - \text{Ga}_{ia} - V_{\text{Ga}2}$	$O_{(2)}$	0.0342 69 a_*	0.0125 21 b	0.0029 89 c	1 1	-27 -20

has to be at least this deep. Our hypothesis is now that the Fermi level position must be such that only the M4 and M1 models are in the EPR active state, while the other variants of the V_{Ga} are not. Since M4 is really the ground state configuration of M1, M4 would then be the preferred model. To establish this possibility we need to examine the transition levels. The calculated positions of the transition levels for different relevant models are shown in Fig. 9 and given numerically in Table V. There is indeed a Fermi level range (as indicated by 'EPR' in Fig. 9) such that only the simple (M1) $V_{\text{Ga}1}$ and the (b)-

TABLE IV. EPR parameters for self-trapped holes, oxygen interstitial and related models. The table is arranged similar to Table III. For further details see the respective caption.

Model	O	g -tensor			HFI	
label structure	type	Δg_1 θ_1 ϕ_1	Δg_2 θ_2 ϕ_2	Δg_3 θ_3 ϕ_3	#Ga	A (G)
M7 STH $h_{O(1)}^+$	$O_{(1)}$	0.0214 90 c	0.0205 0 b	0.0090 90 a_*	2 1	-8 -16
M8 STH $h_{2O(2)}^+$	$2O_{(2)}$	0.0172 0 b	0.0112 90 a_*	0.0042 90 c	2 2 2	-13 -12 -9
M9 O_i	$O_{(1)}+O_i$	0.0283 90 79 c	0.0037 0 b	0.0011 90 -11 a_*	2 1	-8 -19
M10 $O_i - V_{\text{Ga}1}$	O_i	0.0241 90 -84 c	0.0051 0 b	0.0008 90 7 a_*	2	-3

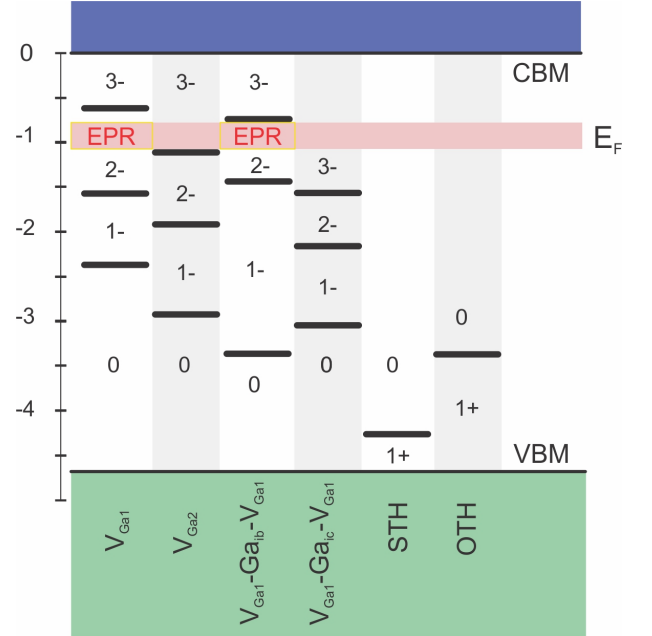


FIG. 9. Transition levels in the gap and expected Fermi level range (in eV) after irradiation, based on which V_{Ga} related centers are EPR active. The $V_{\text{Ga}2}$ level belongs to their tilted spin model M3.

complex (M4) are in the EPR active state. We can see that both the $V_{\text{Ga}1}$ and (b)-complex $V_{\text{Ga}1} - \text{Ga}_{ib} - V_{\text{Ga}1}$ have $2 - / 3-$ levels less deep below the conduction band minimum (CBM) at -0.67 eV and -0.74 eV respectively. It is thus plausible that the $V_{\text{Ga}2}$ and the (c)-complex (M5) are still in the $q = -3$ EPR inactive state if we pin

TABLE V. Transition levels of various defects relative to the conduction band minimum (in eV) and calculated using the hybrid functional.

	V_{Ga1}	V_{Ga2}	(b)-complex	(c)-complex
2-/3-	-0.67	-1.16	-0.74	-1.59
1-/2-	-1.63	-1.91	-1.42	-2.20
0/1-	-2.35	-2.90	-3.34	-3.06

the Fermi level in this range.

The position of all transition levels is somewhat deeper in other calculations reported in the literature.^{10,11,49} The reason for this discrepancy is a different dielectric constant (high-frequency instead of static) used in Deák *et al.*'s procedure¹⁵ for correcting the image charge interactions. Irrespective of this choice, all calculations agree that the V_{Ga2} is deeper than the V_{Ga1} , which is the crucial point needed here. We note that the estimated Fermi level position as indicated in Fig. 9 should not prevent the possibility that the defect catches an additional hole leading to the corresponding $S = 1$ state. Observation of such non-equilibrium states is not uncommon in EPR.

B. Models for EPR2

Next, we consider the possible candidates for EPR2. Now that we have established that the largest g -tensor direction in these defects tends to correspond to the pair of Ga connected to the spin carrying O atom, it becomes clear that few candidates can lead to a g -tensor with maximum along **c**. Only the tilted spin model M3 (V_{Ga2}) is a candidate among the Ga-vacancy type defects. Its spin density and g -tensor and HFI are shown in Fig. 10. The reason is that in this case the directions of the Ga pairs which is in between **b** and **c** become averaged over the two mirror-related pairs on either side of the mirror plane. Note that this applies no matter whether one assumes a static Jahn-Teller effect or a dynamic Jahn-Teller effect. In the former case, there will be some centers in the sample where the spin is on the left and some where it is on the right and the measurement would average over the two.

The hyperfine splitting on the two Ga are not equal for this case because they are inequivalent structurally. For $U = 4$ eV, as given in Table III, they are -21 , -16 G. In hybrid functional they are -33 and -22 G. The above results correspond to the symmetrized case where spin occurs on both sides of the mirror plane and hyperfine then would occur with 2 inequivalent pairs of Ga atoms. Within PBE+ U with $U = 4$ eV, however, the structure actually breaks the symmetry and spin occurs only on one side of the mirror plane. In that case, the difference between the two Ga hyperfine becomes somewhat larger, -25 G, -12.5 G. This is related to a larger difference in bond length of the spin-carrying $\text{O}_{(1)}$ -Ga₍₁₎

and $\text{O}_{(1)}$ -Ga₍₂₎ neighbors which are respectively closer and farther from the mirror-plan. Interestingly, although the O-spin density becomes about a factor two smaller when we split the spin equally over both sides, as is to be expected, the Ga hyperfine changes much less. This illustrates once more that the subtleties of how the wave function spreads to the second neighbor Ga-*s* and hence determines the SHF is not immediately obvious from the overall localization behavior.

The experiments were fit assuming two equivalent Ga and the characteristic fine structure pattern was found to be quite sensitive to relaxing this assumption. However, when we consider that both values are overestimated, their difference may also become smaller in a more sophisticated description including for example dynamic Jahn-Teller effects. One would expect the DJT effect to reduce the difference between the two Ga SHF and smear out the spectrum while explaining nonetheless SHF with only 2 Ga atoms. The average value of the two inequivalent Ga is a bit smaller than for the EPR1 model, which is consistent with the experimental observation. Upon close examination, one may notice that for EPR2 the details of the SHF structure are a bit less resolved than for EPR1 because they show similar broadening but a smaller splitting. Thus a small difference between the two Ga hyperfine cannot be excluded. Future experimental work using higher microwave frequency might be able to reveal the difference between the two Ga.

In terms of the g -tensor, this model has the largest value along **c** in agreement with experiment, but the next smaller value is along **a*** rather than **b**. This small deviation from experiment may be considered to fall within the error of the calculations. Thus, M3 appears to be a reasonable model for EPR2 but not perfect.

Next, we discuss some of the alternative models based on self-trapped holes (STH) or oxygen interstitial (O_i). First we consider the M7 self-trapped hole model with the hole trapped on $\text{O}_{(1)}$ which was previously proposed to be the origin of this spectrum.²³ Its g -tensor has indeed principal value directions close to **c**, followed by **b** and **a***, however with values of $g_c \approx g_b \gg g_{a^*}$. More importantly, there is strong hyperfine interaction with three Ga and the strongest component is actually on the third single Ga. The next model M8 with holes trapped on two adjacent $\text{O}_{(2)}$ has hyperfine with 6 Ga and not matching g -tensor and can, thus, easily be dismissed. A figure for this model can be found in Supplementary Information.⁵⁰

The O_i model M9 on the other hand (shown in Fig. 12) has a g -tensor that matches the experiment quite well in terms of the order of the principal axes, $g_c \gg g_b \approx g_{a^*}$ although Δg_c is still a bit small. However, the HFI is not in good agreement with experiment because three Ga atoms have significant HFI, an equivalent pair with value of -8 G and a third one with a higher value of -19 G. Note that the values with the pair are significantly lower than for the V_{Ga} . However, we cannot ignore the interaction with the third Ga because it is in fact the higher HFI. As can be seen in Fig. 12, the strong HFI

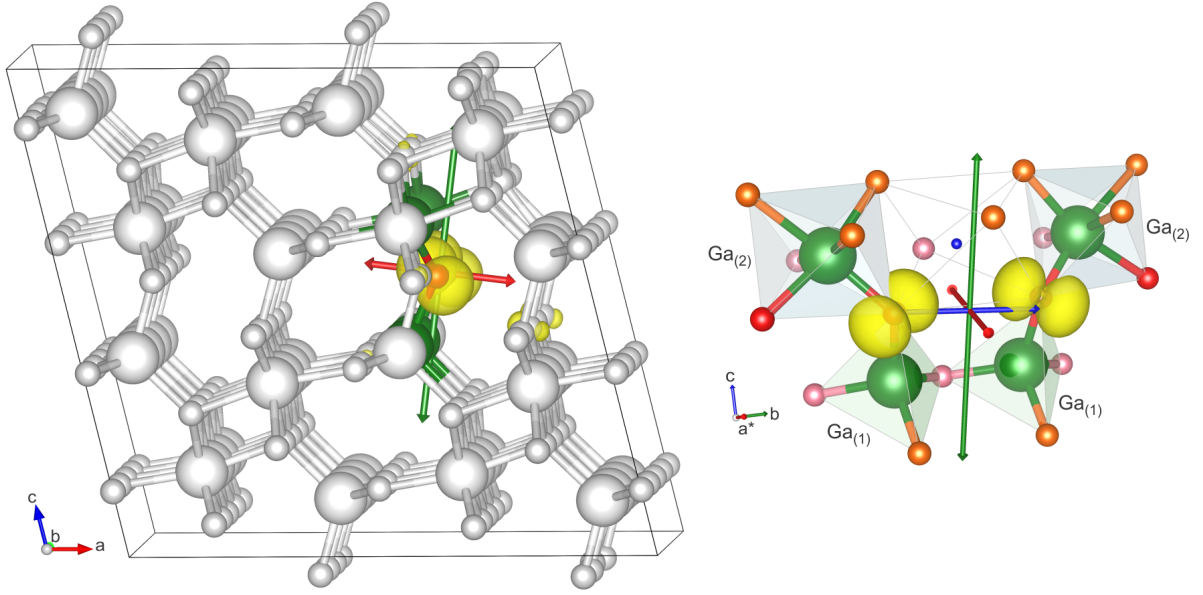


FIG. 10. Model M3 with tilted spins for $V_{\text{Ga}2}$ structure, spin density, g -tensor and Ga atoms with strong HFI. Details as in Fig. 6. Note that this is a symmetrized model in which spin appears to occur on both sides of the mirror plane of the defect. When relaxing this structure without symmetry constraint, the tilted spin occurs only on one side so that there is only hyperfine interaction with two Ga but the left and right variant would give the same c -oriented major axis of the g -tensor.

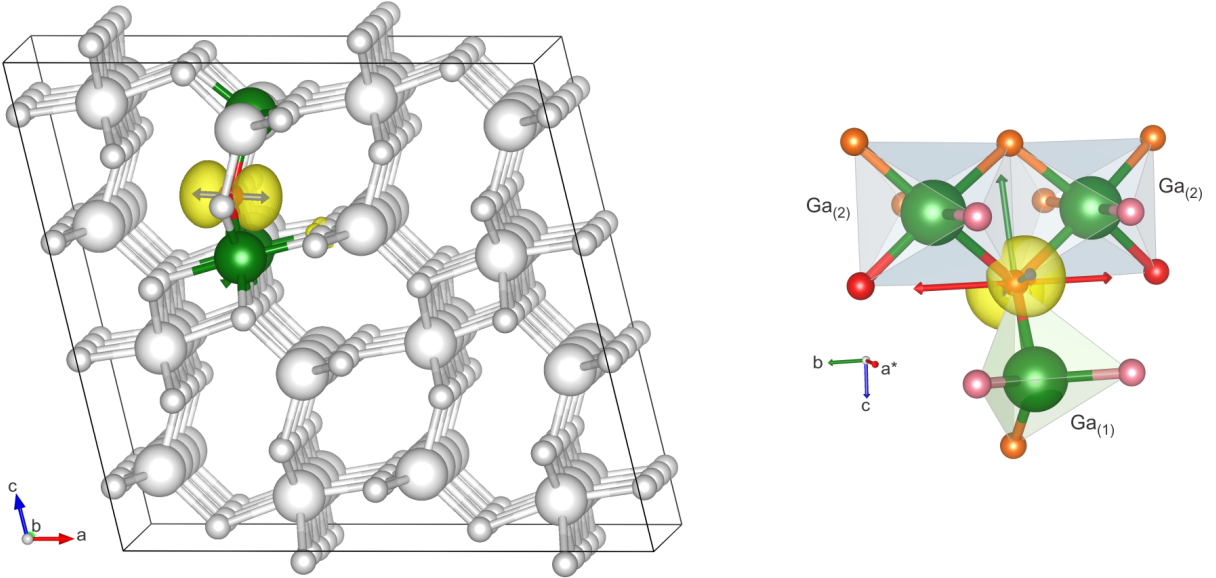


FIG. 11. Self-trapped polaron spin density on $O_{(1)}$ (Model M7) in yellow, g -tensor (double arrows) and Ga exhibiting strong HFI. Details as in Fig. 6

with the third Ga results from the spin density to be in a π -like orbital spread over the two O atoms in the dumbbell, as is to be expected. So, this model has the g -tensor which best matches the experiment but should be ruled out because it would predict HFI with a prominent third Ga which would definitely change the fine structure sufficiently to be detected experimentally.

As a further modification of this model, we removed

the third Ga from M9 and thereby created model M10 ($O_i - V_{\text{Ga}1}$), shown in Supplementary Information.⁵⁰ In that case, the spin becomes more pulled toward the O farther away from the $\text{Ga}_{(2)}$ pair, the g -tensor stays similar but the HFI on the pair of equivalent Ga becomes much too small. These two O_i models M9/M10 were relaxed only within DFT+ U .

Finally, referring back to Fig. 9 we note that the self-

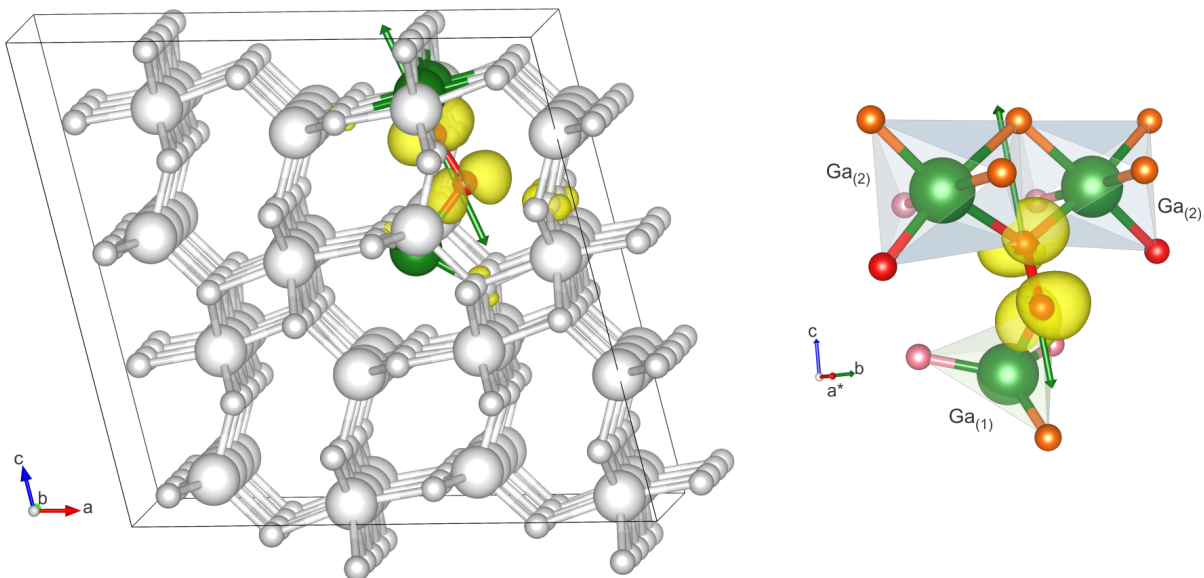


FIG. 12. Interstitial O_i with O-O dumbbell oriented along \mathbf{c} (M9) structure, spin density in yellow, g -tensor (double arrows) and Ga exhibiting strong HFI. Details as in Fig. 6

trapped holes (STH, models M7/M8) as well as the split-interstitial O_i models (M9/M10) have much deeper transition levels to the EPR active positive charge states. While this does not completely exclude them under optical excitation, it makes them much less likely candidates.

C. $S = 1$ spectra

Several of the defects were calculated in the $q = -1$ state in order to assign the $S = 1$ spectra. It was found that for the simple $V_{\text{Ga}1}$ model, the second hole tends to localize on the pair of $O_{(2)}$ rather than the $O_{(3)}$ on the mirror plane. This would break the symmetry and not be consistent with an $S = 1$ very closely related to the $S = 1/2$ EPR1 spectrum. Similar considerations hold for $V_{\text{Ga}2}$ when starting from the symmetric solution with spin on $O_{(2)}$ on the mirror plane (M2). On the other hand, the $V_{\text{Ga}1}-\text{Ga}_{ib}-V_{\text{Ga}1}$ (M4 model), which we already consider as the most likely model for EPR1, is an ideal candidate for the $S = 1$ spectrum. First, the spins on the $O_{(1)}$ type atoms near each $V_{\text{Ga}1}$ in this model are far apart (~ 7.2 Å) so that this would indeed correspond to two weakly interacting spins. Second, this $S = 1$ $q = -1$ state was indeed found to have halved hyperfine interactions compared to the $S = 1/2$ and a similar g -tensor with maximum along \mathbf{b} of $\Delta g_1 = 0.0316$, $\Delta g_2 = 0.014$ close to (about 17° from) the \mathbf{c} -axis and $\Delta g_3 = 0.007$ close to \mathbf{a}^* . Third, this particular complex has lowest energy among all the Ga-vacancy related models in the $q = -1$ charge state (See Table II).

Next, let us analyze the size of the the zero-field splitting. The point dipole-dipole interaction between two

$S = 1/2$ spins is given by

$$U_{12}(\mathbf{r}) = \frac{\mu_0}{4\pi} \frac{[\mathbf{m}_1 \cdot \mathbf{m}_2 - 3(\mathbf{m}_1 \cdot \hat{\mathbf{r}})(\mathbf{m}_2 \cdot \hat{\mathbf{r}})]}{r^3} \quad (3)$$

The splitting between the two parts of the $S = 1$ spectrum is $2D$ and can be set equal to this energy difference if we assume that the angular factors stay close to 1. Using $m_i = g_e \mu_B \sqrt{S(S+1)}$ the D value then corresponds to a distance d between the two $S = 1/2$ of 5.4 Å. This agrees with the estimate by Kananen *et al.*²² The distance between the two spin-carrying O atoms in the M4 model is 7.2 Å. However, the point dipole model is not sufficient to determine the distance accurately to better than a few Å because in a quantum mechanical calculations, one would need to determine the expectation value of the dipole interaction for the particular defect wave function of O- p orbital.⁵¹ Thus the observed value is consistent with the model within the error bars of the point dipole model. The direction of the axial zero-field splitting also agrees reasonably well with the vector linking the two O atoms in the M4 model. We conclude that the occurrence of this $S = 1$ spectrum and its characteristics provides further strong confirmation to our identification of EPR1 with the (b)-complex form of the $V_{\text{Ga}1}$.

As for the EPR2 related $S = 1$ state, the M3 model is also a plausible model to catch a second hole. We found the $S = 1$ state of M3 with $q = -1$ to have a similar g -tensor: $\Delta g_1 = 0.037$, $\theta_1 = 90^\circ$, $\phi_1 = 56^\circ$, close to \mathbf{c} -axis, $\Delta g_2 = 0.0245$, $\theta = 0$ (\mathbf{b} -axis), and $\Delta g_3 = 0.0154$, $\theta_3 = 90^\circ$, $\phi_3 = -34^\circ$ (closer to \mathbf{a}_*) as the corresponding $S = 1/2$ model. However, there is somewhat larger interaction between the spins in this model because the O are only 3.5 Å apart. This leads to a somewhat larger difference between the nonequivalent Ga atoms which now

have hyperfine contact terms of -12 G and -27 G instead of -16 G and -21 G in the $S = 1/2$. This is less clearly indicative of weakly coupled spins. We note also that this newly found EPR2 $S = 1$ spectrum has a more complex lineshape with a broad line underlying the halved hyperfine splitting of the $S = 1/2$ part of the spectrum. This broadening could possibly be explained by the two sets of slightly inequivalent pairs involved in this spectrum. The smaller distance is compatible with a larger zero field splitting although the scaling with d^{-3} would have suggested a larger difference. Using the above approach, the $D = 322$ MHz corresponds to 4.9 Å instead of the 3.5 Å distance between the spins in the M3 model. We note once more that the point dipole-dipole interaction provides only an approximate model for the zero-field splitting⁵¹ and also ignores the additional exchange interaction between the spins, which might play a more significant role for these closer spins. The axis of the axial D does in this case not correspond to the line joining the two O atoms but does lie in the symmetry plane of the defect as expected for an axial $S = 1$ center.

On the other hand, the O_i is very unlikely to have an associated $S = 1$ $q = +2$ charge state. The $q = +2$ state can safely be dismissed on the ground of total energy calculations. This is another reason why this is a less attractive model for EPR2.

D. Photoexcitation process

Finally, the nature of the photoexcitation process and the meaning of the threshold value are discussed. If we consider the EPR2 to be related to $V_{\text{Ga}2}$ in the M3 model, we may consider a migration path of Ga for converting the M4 model to M3. Following Ref. 49 the migration barrier for from Ga in the interstitial i_b site to a $\text{Ga}_{(1)}$ site via a $q9$ jump is 1.0 eV in the $q = -2$ charge state. (We follow here the notations of Kyrtos *et al.*⁴⁹.) We are then left with a single $V_{\text{Ga}1}$, which could migrate to one of the neighboring octahedral sites by a $q6$, $q8$, $q10$ or $q4+q5$ paths. These would add an additional 1.2 - 1.7 eV. So, the total energy to transform the M4 to a $V_{\text{Ga}2}$ path would amount to about 2.5 ± 0.3 eV. This agrees rather well with the phototreshold. Also, within this process the defect configuration giving rise to EPR1 is expected to disappear at the same time as the configuraton giving EPR2 appears. In the above model, the photoexcitation process is viewed as a direct transformation of the defect from one form to the other related to V_{Ga} migration.

We could also view the photoexcitation process as transferring a hole form an M4 model to an already existing nearby octahedral vacancy which is still in the EPR inactive state. Or alternatively, the electron is transferred from the octahedral to the tetrahedral vacancy in its complex M4 configuration. This would also simultaneously activate the octahedral vacancy EPR signal and deactivate the M4 one as is observed to be the case.

We should however keep in mind that this EPR center

can also be created by X-ray absorption at low temperature starting from the EPR1 containing sample.²³ So, the meaning of the phototreshold energy is not entirely clear.

VIII. CONCLUSIONS

In this paper, we provided experimental details of the EPR spectra previously reported only briefly.²⁴ In particular, we found that each spectrum is accompanied by a corresponding $S = 1$ spectrum. More importantly, we provide here the full detail of the calculations which leads to our assignment of the EPR spectra to specific defect configurations. When we allow for the still somewhat limited accuracy of PBE-calculated g -tensor values and focus on the main qualitative features, such as the orientations of the principal axes of the g -tensor relative to the crystal axes, and the number of Ga atoms on which hyperfine interaction is found to be strong, a clear picture emerges. The EPR1 spectrum most likely corresponds to the $V_{\text{Ga}1} - \text{Ga}_{ib} - V_{\text{Ga}1}$ model, which is in fact the ground state of $V_{\text{Ga}1}$ in the EPR relevant $q = -2$ charge state. The reason why other forms of the $V_{\text{Ga}1}$ or the octahedral $V_{\text{Ga}2}$ are not seen in the experiment is that they are still in the EPR inactive $q = -3$ charge state even after the Fermi level is somewhat lowered compared to the as grown crystal after the irradiation treatment. This explanation is consistent with the calculated transition levels, which is indeed found to be less deep below the conduction band for the $V_{\text{Ga}1} - \text{Ga}_{ib} - V_{\text{Ga}1}$ model and with a plausible assignment of the Fermi level in these samples based on the observation of the Fe^{3+} EPR signal.

For EPR2, the EPR center found after photoexcitation, the titled spin $V_{\text{Ga}2}$ emerges as the most likely model. While it agrees less closely with experimental values than for EPR1, the alternatives considered here, such as the self-trapped hole or a split interstitial oxygen could all be ruled out based on various detailed arguments but mostly because they would clearly show hyperfine interaction on three Ga atoms and are much less likely to be in an EPR active charge state and cannot support a corresponding $S = 1$ center.

The hyperfine interaction for both models was found to be somewhat overestimated even when including Hubbard- U corrections to the GGA density functional or using a hybrid functional. This indicates that calculating hyperfine interactions constitutes a very demanding test on the accuracy of the defect wave function. Another possible explanation for this discrepancy could be the occurrence of a dynamic Jahn-Teller effect which may lead to a reduction of the hyperfine interaction. This effect would apply to both of the here proposed models which both correspond to a symmetry broken electronic state of the rather complex defect.

While the overestimate of the HFI certainly deserves further investigation as well as the dynamical Jahn-Teller effect, it is not a crucial point in our assignment of the

most plausible models to the spectra. This identification is mostly based on qualitative features, such as the direction of the major axis of the g -tensor, the number of Ga atoms which show hyperfine interaction, the likelihood of the different models to be in the EPR active states based on their transition levels and the capability of the defect to capture a second hole leading to the corresponding $S = 1$ spectra. These aspects are robust and not sensitive to details of the calculation method. Finally, we note that our identification of the EPR1 center with the $V_{\text{Ga}1} - \text{Ga}_{ib} - V_{\text{Ga}1}$ model provides an experimental confirmation of this interesting configuration of the Ga-vacancy in $\beta\text{-Ga}_2\text{O}_3$. Also, although we here focused on identifying the until now experimentally observed EPR spectra, the predictions for other defect models may become extremely useful in future experimental investigations of these materials, in particular those with modified

Fermi level.

ACKNOWLEDGMENTS

The work at CWRU was supported by the National Science Foundation under grant No. DMR-1708593. The calculations were carried out at the Ohio Supercomputer Center under Project No. PDS0145. The work at BC-CMS was supported by the DFG grant No. FR2833/63-1 and by the Supercomputer Center of Northern Germany (HLRN Grant No. hbc00027). U.G. acknowledges support by the Deutsche Forschungsgemeinschaft (DFG) priority program SPP-1601. We acknowledge the Helmholtz Zentrum Dresden (HZDR) in Rossendorf (Germany) for the proton and electron irradiation and the laboratory CEMHTI, CNRS, Orleans (France) for proton irradiation.

- ¹ K. Sasaki, M. Higashiwaki, A. Kuramata, T. Masui, and S. Yamakoshi, *J. Cryst. Growth* **378**, 591 (2013), the 17th International Conference on Molecular Beam Epitaxy.
- ² T. Matsumoto, M. Aoki, A. Kinoshita, and T. Aono, *Jap. J. Appl. Phys.* **13**, 1578 (1974).
- ³ H. Peelaers and C. G. Van de Walle, *Phys. Status Solidi (b)* **252**, 828 (2015).
- ⁴ J. Furthmüller and F. Bechstedt, *Phys. Rev. B* **93**, 115204 (2016).
- ⁵ K. A. Mengle, G. Shi, D. Bayerl, and E. Kioupakis, *Appl. Phys. Lett.* **109**, 212104 (2016), <http://dx.doi.org/10.1063/1.4968822>.
- ⁶ A. Ratnaparkhe and W. R. L. Lambrecht, *Applied Physics Letters* **110**, 132103 (2017), <http://dx.doi.org/10.1063/1.4978668>.
- ⁷ A. J. Green, K. D. Chabak, E. R. Heller, R. C. Fitch, M. Baldini, A. Fiedler, K. Irmscher, G. Wagner, Z. Galazka, S. E. Tetlak, A. Crespo, K. Leedy, and G. H. Jessen, *IEEE Electron Device Letters* **37**, 902 (2016).
- ⁸ B. J. Baliga, *IEEE Electron Device Letters* **10**, 455 (1989).
- ⁹ H. Peelaers, D. Steiauf, J. B. Varley, A. Janotti, and C. G. Van de Walle, *Phys. Rev. B* **92**, 085206 (2015).
- ¹⁰ J. B. Varley, H. Peelaers, A. Janotti, and C. G. Van de Walle, *J. Phys. Condens. Matter* **23**, 334212 (2011).
- ¹¹ J. B. Varley, A. Janotti, C. Franchini, and C. G. Van de Walle, *Phys. Rev. B* **85**, 081109 (2012).
- ¹² T. Harwig and F. Kellendonk, *J. Solid State Chem.* **24**, 255 (1978).
- ¹³ T. Zacherle, P. C. Schmidt, and M. Martin, *Phys. Rev. B* **87**, 235206 (2013).
- ¹⁴ H. Peelaers and C. G. Van de Walle, *Phys. Rev. B* **94**, 195203 (2016).
- ¹⁵ P. Deák, Q. Duy Ho, F. Seemann, B. Aradi, M. Lorke, and T. Frauenheim, *Phys. Rev. B* **95**, 075208 (2017).
- ¹⁶ M. E. Ingebrigtsen, J. B. Varley, A. Y. Kuznetsov, B. G. Svensson, G. Alfieri, A. Mihaila, U. Badstübner, and L. Vines, *Applied Physics Letters* **112**, 042104 (2018), <https://doi.org/10.1063/1.5020134>.
- ¹⁷ K. Irmscher, Z. Galazka, M. Pietsch, R. Uecker, and R. Fornari, *Journal of Applied Physics* **110**, 063720 (2011), <https://doi.org/10.1063/1.3642962>.
- ¹⁸ Z. Zhang, E. Farzana, A. R. Arehart, and S. A. Ringel, *Applied Physics Letters* **108**, 052105 (2016), <https://doi.org/10.1063/1.4941429>.
- ¹⁹ M. E. Ingebrigtsen, A. Y. Kuznetsov, B. G. Svensson, G. Alfieri, A. Mihaila, U. Badstbner, A. Perron, L. Vines, and J. B. Varley, *APL Materials* **7**, 022510 (2019), <https://doi.org/10.1063/1.5054826>.
- ²⁰ H. Gao, S. Muralidharan, N. Pronin, M. R. Karim, S. M. White, T. Asel, G. Foster, S. Krishnamoorthy, S. Rajan, L. R. Cao, M. Higashiwaki, H. von Wenckstern, M. Grundmann, H. Zhao, D. C. Look, and L. J. Brillson, *Applied Physics Letters* **112**, 242102 (2018), <https://doi.org/10.1063/1.5026770>.
- ²¹ M. M. Islam, D. Rana, A. Hernandez, M. Haseman, and F. A. Selim, *Journal of Applied Physics* **125**, 055701 (2019), <https://doi.org/10.1063/1.5066424>.
- ²² B. E. Kananen, L. E. Halliburton, K. T. Stevens, G. K. Foundos, and N. C. Giles, *Applied Physics Letters* **110**, 202104 (2017), <http://dx.doi.org/10.1063/1.4983814>.
- ²³ B. E. Kananen, N. C. Giles, L. E. Halliburton, G. K. Foundos, K. B. Chang, and K. T. Stevens, *Journal of Applied Physics* **122**, 215703 (2017), <https://doi.org/10.1063/1.5007095>.
- ²⁴ H. J. von Bardeleben, S. Zhou, U. Gerstmann, D. Skachkov, W. R. L. Lambrecht, Q. D. Ho, and P. Deák, *APL Materials* **7**, 022521 (2019), <https://doi.org/10.1063/1.5053158>.
- ²⁵ S. Geller, *J. Chem. Phys.* **33**, 676 (1960), <http://dx.doi.org/10.1063/1.1731237>.
- ²⁶ J. P. Perdew, M. Ernzerhof, and K. Burke, *J. Chem. Phys.* **105**, 9982 (1996).
- ²⁷ J. Heyd, G. E. Scuseria, and M. Ernzerhof, *J. Chem. Phys.* **118**, 8207 (2003).
- ²⁸ J. Heyd, G. E. Scuseria, and M. Ernzerhof, *J. Chem. Phys.* **124**, 219906 (2006).
- ²⁹ G. Kresse and J. Furthmüller, *Computational Materials Science* **6**, 15 (1996).

- ³⁰ G. Kresse and D. Joubert, *Phys. Rev. B* **59**, 1758 (1999).
- ³¹ <https://www.vasp.at/>.
- ³² C. J. Pickard and F. Mauri, *Phys. Rev. B* **63**, 245101 (2001).
- ³³ C. J. Pickard and F. Mauri, *Phys. Rev. Lett.* **88**, 086403 (2002).
- ³⁴ P. Giannozzi, S. Baroni, N. Bonini, M. Calandra, R. Car, C. Cavazzoni, D. Ceresoli, G. L. Chiarotti, M. Cococcioni, I. Dabo, A. Dal Corso, S. de Gironcoli, S. Fabris, G. Fratesi, R. Gebauer, U. Gerstmann, C. Gougousis, A. Kokalj, M. Lazzeri, L. Martin-Samos, N. Marzari, F. Mauri, R. Mazzarello, S. Paolini, A. Pasquarello, L. Paulatto, C. Sbraccia, S. Scandolo, G. Sclauzero, A. P. Seitsonen, A. Smogunov, P. Umari, and R. M. Wentzcovitch, *Journal of Physics: Condensed Matter* **21**, 395502 (19pp) (2009).
- ³⁵ J. P. Perdew, K. Burke, and M. Ernzerhof, *Phys. Rev. Lett.* **77**, 3865 (1996).
- ³⁶ H. J. von Bardeleben, J. L. Cantin, U. Gerstmann, A. Scholle, S. Greulich-Weber, E. Rauls, M. Landmann, W. G. Schmidt, A. Gentils, J. Botsoa, and M. F. Barthe, *Phys. Rev. Lett.* **109**, 206402 (2012).
- ³⁷ H. J. von Bardeleben, J. L. Cantin, H. Vrielinck, F. Callens, L. Binet, E. Rauls, and U. Gerstmann, *Phys. Rev. B* **90**, 085203 (2014).
- ³⁸ G. Pfanner, C. Freysoldt, J. Neugebauer, and U. Gerstmann, *Phys. Rev. B* **85**, 195202 (2012).
- ³⁹ B. M. George, J. Behrends, A. Schnegg, T. F. Schulze, M. Fehr, L. Korte, B. Rech, K. Lips, M. Rohrmüller, E. Rauls, W. G. Schmidt, and U. Gerstmann, *Phys. Rev. Lett.* **110**, 136803 (2013).
- ⁴⁰ M. Rohrmüller, W. G. Schmidt, and U. Gerstmann, *Phys. Rev. B* **95**, 125310 (2017).
- ⁴¹ M. Cococcioni and S. de Gironcoli, *Phys. Rev. B* **71**, 035105 (2005).
- ⁴² I. Timrov, N. Marzari, and M. Cococcioni, *Phys. Rev. B* **98**, 085127 (2018).
- ⁴³ Q. D. Ho, T. Frauenheim, and P. Deák, *Journal of Applied Physics* **124**, 145702 (2018), <https://doi.org/10.1063/1.5049861>.
- ⁴⁴ F. S. Ham, *Phys. Rev.* **138**, A1727 (1965).
- ⁴⁵ A. Mauger, H. J. von Bardeleben, J. C. Bourgoin, and M. Lannoo, *Phys. Rev. B* **36**, 5982 (1987).
- ⁴⁶ <http://qe-forge.org/gf/project/qe-gipaw/>.
- ⁴⁷ S. Blügel, H. Akai, R. Zeller, and P. H. Dederichs, *Phys. Rev. B* **35**, 3271 (1987).
- ⁴⁸ C. G. Van de Walle and P. E. Blöchl, *Phys. Rev. B* **47**, 4244 (1993).
- ⁴⁹ A. Kyrtsov, M. Matsubara, and E. Bellotti, *Phys. Rev. B* **95**, 245202 (2017).
- ⁵⁰ The Supplementary Information contains additional figures of the spin density, g -tensor and large hyperfine atoms for some of the models, not shown in the main text. Also VESTA files which allow to view these structures from different angles are provided.
- ⁵¹ C. Riplinger, J. P. Y. Kao, G. M. Rosen, V. Kathirvelu, G. R. Eaton, S. S. Eaton, A. Kutateladze, and F. Neese, *Journal of the American Chemical Society* **131**, 10092 (2009), PMID: 19621964, <https://doi.org/10.1021/ja901150j>.